

Rotation Averaging: A Primal-Dual Method and Closed-Forms in Cycle Graphs

Gabriel Moreira, Manuel Marques, and João Paulo Costeira

Abstract—A cornerstone of geometric reconstruction, rotation averaging seeks the set of absolute rotations that optimally explains a set of measured relative orientations between them. In addition to being an integral part of bundle adjustment and structure-from-motion, the problem of synchronizing rotations also finds applications in visual simultaneous localization and mapping, where it is used as an initialization for iterative solvers, and camera network calibration. Nevertheless, this optimization problem is both non-convex and high-dimensional. In this paper, we address it from a maximum likelihood estimation standpoint and make a twofold contribution. Firstly, we set forth a novel primal-dual method, motivated by the widely accepted spectral initialization. Further, we characterize stationary points of rotation averaging in cycle graphs topologies and contextualize this result within spectral graph theory. We benchmark the proposed method in multiple settings and certify our solution via duality theory, achieving a significant gain in precision and performance.

Index Terms—Rotation Averaging, Pose Graph Optimization, Visual SLAM



1 INTRODUCTION

POSE graph optimization (PGO), synchronization over the Euclidean group and motion averaging are designations often used when referring to the problem of finding the optimal configuration of a set of vertices, given a set of corrupted relative pairwise measurements between them. What the aforementioned vertices represent varies according to the application. In Robotics, the most natural use of PGO is in Visual Simultaneous Localization and Mapping (SLAM), where each vertex corresponds to the pose of a robot at a given instant [1], [2], [3], [4]. Variants of PGO over $SO(3)$, known as rotation averaging [5], and over the complex circle group, defined as phase synchronization [6], have been extensively studied as well. The former usually linked to 3D reconstruction applications in Computer Vision tasks such as structure-from-motion (SfM) [7], bundle-adjustment and camera network calibration [8], while the latter finds applications in signal processing and distributed networks e.g., clock synchronization.

In this paper, we build on the MLE formulation of PGO [2], [9], making a two-fold contribution. We characterize the stationary points in $SO(p)$, for cycle graph topologies and leverage recent results on the SDP dual problem and strong duality to propose a primal-dual method with spectral updates, akin to a recursive spectral initialization [10]. We prove that our method is globally optimal in cycle graphs and rely on the dual SDP certificate for an empirical optimality assessment in the general case. This is accomplished via numerous experiments using well known PGO benchmark datasets [1], [2].

An overview of PGO

In general, the problem may be defined as follows. Let $G = (\mathcal{V}, \mathcal{E})$ be a graph. Define \mathcal{S} as the feasible set, which we can assume to be a group. Each pairwise tuple $(i, j) \in \mathcal{V}^2$, is identified with the composition of x_i with x_j^{-1} i.e., $x_{ij} := x_i x_j^{-1}$, which may be interpreted as the value of i relative to that of j . Given a set of noisy measurements of these relative values \tilde{x}_{ij} , $(i, j) \in \mathcal{E}$, PGO may be formally defined as

$$\begin{aligned} & \underset{x_1, \dots, x_n}{\text{minimize}} && \sum_{(i,j) \in \mathcal{E}} d(x_i x_j^{-1}, \tilde{x}_{ij}) \\ & \text{subject to} && x_i \in \mathcal{S}, \quad i = 1, \dots, n \end{aligned} \quad (1)$$

where $d(\cdot, \cdot)$ is an appropriate distance function in \mathcal{S} . Consider the example of letting \mathcal{S} be the group of translations \mathbb{T} of \mathbb{R}^p . Leveraging the isomorphism between \mathbb{T} and \mathbb{R}^p itself and letting d define the norm induced by the usual inner product of \mathbb{R}^p , Problem (1) involves just the minimization of the least-squares cost $\sum_{(i,j) \in \mathcal{E}} \|(t_i - t_j) - \tilde{t}_{ij}\|_2^2$, whose closed-form solution is, in general, given by

$$T = J^\dagger \tilde{T}, \quad (2)$$

where J is the signed incidence matrix of G , the i -th row of T contains t_i^\top and the k -th row of \tilde{T} contains \tilde{t}_k^\top . We may check that the solution given by (2) verifies

$$t_i^* = \arg \min_{t \in \mathbb{R}^p} \sum_{j: (i,j) \in \mathcal{E}} \|(t - t_j^*) - \tilde{t}_{ij}\|_2^2, \quad (3)$$

for all $i \in \mathcal{V}$. Each vertex is thus in consensus with its neighbors regarding its own position. This can be observed in Fig. 1, where we add an incorrect measurement (diagonal in black) to a noiseless graph with a mesh-like topology (on the left). The inconsistency introduced by the diagonal measurement diffuses through the graph (shown on the right), spreading between adjacent vertices. If we allow the edges of the mesh to represent springs with the equal stiffness, the solution is the state of equilibrium of the system, after the

- *G Moreira is with the LTI, Carnegie Mellon University, Pittsburgh, PA 15213 and with the Institute for Systems and Robotics, Instituto Superior Técnico, Lisboa 1049-001, Portugal. E-mail: gmoreira@cs.cmu.edu*
- *M Marques and JP Costeira are with the Institute for Systems and Robotics, Instituto Superior Técnico, Lisboa 1049-001, Portugal.*

arXiv:2406.18564v1 [cs.CV] 29 May 2024

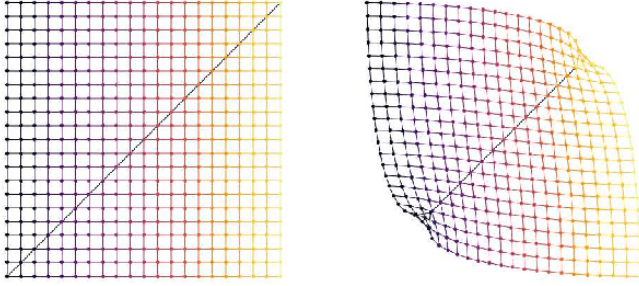


Fig. 1. Left: ground-truth graph consisting of a mesh with 441 vertices. Edges of this colored grid correspond to noiseless pairwise measurements. One diagonal measurement (black) is added, which underestimates the true diagonal by 70%. Right: optimized vertex positions.

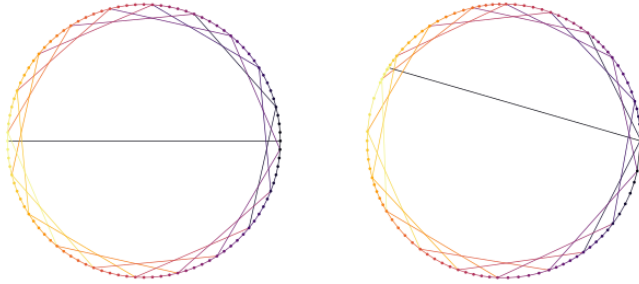


Fig. 2. Left: ground-truth graph, with 100 vertices represented on the complex circle group. Colored edges correspond to noiseless measurements. The horizontal black measurement is added, with a phase error of $-\pi/4$ over the ground-truth π . Right: vertex positions of the phase synchronization global optimum.

diagonal spring, with nominal length smaller than the mesh diagonal is added to the system. In this case, PGO has thus an interesting interpretation of error redistribution, which can be described from a graph consensus standpoint or in terms of an elastic spring system.

PGO's main difficulty arises when rotations are introduced, making \mathcal{S} non-convex and ultimately rendering the problem less tractable. In Fig. 2, a graph over the complex circle group is shown. Once again, the colored edges correspond to noiseless measurements and the horizontal black line to an edge whose measurement has an angular error of $-\pi/4$. The problem has multiple local minima i.e., there are multiple equilibrium states for this system. The optimum is shown on the right. Remarkably, the reasoning behind our Euclidean example of Fig. 1 is still valid i.e., the optimal rotations will be in consensus with their neighbors,

$$R_i^* = \arg \min_{R \in \text{SO}(p)} \sum_{j: (i,j) \in \mathcal{E}} \|\tilde{R}_{ij} R_j^* - R\|_F^2, \quad (4)$$

for all $i \in \mathcal{V}$. While the optimization problem in (4) can be solved in closed-form via a Singular Value Decomposition (SVD), the overall synchronization problem is not as tractable. In fact, under the maximum likelihood formulation pervasive in the literature, which is an instance of (1), PGO in $\text{SE}(p)$ and $\text{SO}(p)$ is a variant of the max-cut problem, known as orthogonal cut and similarly to the former, it is itself NP-hard [11]. Akin to max-cut, PGO also admits a convex relaxation under the form of a Semidefinite

Program (SDP), which is its bi-dual. Characterizing the tightness of this relaxation, which is desirable from an optimality certification standpoint, has been the subject of recent research [12], [13].

In the subsequent sections, we start by reviewing some of the recent works in PGO and general synchronization. In Section 4, we state our hypothesis and define the problem. We put forward our primal-dual method for the rotation synchronization problem in Section 5 and analyze stationary points in cycle graphs in Section 6. Empirical validation and benchmarks are present subsequently. This work is an extension of the conference paper [14].

2 NOTATION

We use \mathbb{R} and \mathbb{C} to denote the real and complex numbers, respectively. The trace operator reads as $\text{tr}(\cdot)$. The usual inner product on \mathbb{R}^p is denoted as $\langle \cdot, \cdot \rangle$ i.e., $\langle A, B \rangle = \text{tr}(A^\top B)$ and the operator norm thereby induced via $\|\cdot\|_2$. The Frobenius norm is written as $\|\cdot\|_F$. We denote the $p \times p$ identity matrix by I_p and the null matrix by 0_p . Positive definite and semidefinite matrices are indicated via $A \succ 0$ and $A \succeq 0$, respectively. As we will be dealing with block matrices and vectors, subscripts A_{ij} are used to indicate matrix blocks and V_i , vector blocks, respectively. In the case of iterates, we use parentheses as $A_{(k)}$ to indicate the k -th iteration.

Throughout this paper, we will be considering Euclidean transformations of \mathbb{R}^p . More concretely, targeting applications where $p = 3$. The orthogonal group can be realized as the matrix group

$$O(p) = \{R \in \mathbb{R}^{p \times p} \mid R^\top R = RR^\top = I\}, \quad (5)$$

and the special orthogonal group as the connected component of $O(p)$ with positive determinant

$$\text{SO}(p) = \{R \in \mathbb{R}^{p \times p} \mid R \in O(p), \det(R) = 1\}. \quad (6)$$

The Special Euclidean group is defined as

$$\text{SE}(p) = \{t \in \mathbb{R}^p, R \in \text{SO}(p) \mid (t, R)\}. \quad (7)$$

We borrow some linear operators defined in [13], that vastly simplify the notation, namely Diag and BlockDiag . Given a $p \times p$ -block matrix $U \in \mathbb{R}^{np \times np}$, BlockDiag extracts the block diagonal

$$\text{BlockDiag}(U) = \begin{bmatrix} U_{11} & \dots & 0 \\ \vdots & \ddots & \vdots \\ 0 & \dots & U_{nn} \end{bmatrix}. \quad (8)$$

Conversely, Diag , forms a $np \times np$ block diagonal matrix from a set of n blocks of dimension $p \times p$

$$\text{Diag}(U_1, \dots, U_n) = \begin{bmatrix} U_1 & \dots & 0 \\ \vdots & \ddots & \vdots \\ 0 & \dots & U_n \end{bmatrix}. \quad (9)$$

Finally, let us recall some elements of graph theory. We refer to graphs as $G = (\mathcal{V}, \mathcal{E})$, with $\mathcal{V} = \{1, \dots, |\mathcal{V}|\}$ the set of vertices and $\mathcal{E} = \{e_1, \dots, e_{|\mathcal{E}|}\} \subseteq \mathcal{V} \times \mathcal{V}$ the set of edges. Here, $|\cdot|$ indicates the cardinality of the respective set. While we identify each graph vertex with an integer, every edge

$e_k \in \mathcal{E}$ is identified with a tuple consisting of its incident vertices. Thus, the edge from vertex i to j will henceforth be indicated by the tuple (i, j) . The set of neighbors of a vertex i is denoted as δ_i . The degree of a vertex $i \in V$ is the number of its neighbors and it is therefore written as $|\delta_i|$. A weighted graph is a graph wherein we have a real-valued function w defined on the set of edges as w_{ij} . By comparison, in an unweighted graph we assume this function to be identically 1. From the set of edge weights we can define the graph's adjacency matrix $A \in \mathbb{R}^{|\mathcal{V}| \times |\mathcal{V}|}$ as

$$A_{ij} := \begin{cases} w_{ij}, & (i, j) \in \mathcal{E} \\ 0, & \text{otherwise} \end{cases} \quad (10)$$

and the graph Laplacian as $L := \text{Diag}(\delta_1, \dots, \delta_{|\mathcal{V}|}) - A$.

3 RELATED WORK

Research on PGO has undergone a remarkable evolution. In this section, we hope to shed light on a set of the works that have contributed towards it. Keeping in line with the theme of this article, we will focus on the Maximum Likelihood Estimation (MLE) formulation of synchronization problem on $SO(p)$. For a review of robust synchronization, the reader is referred to [15], [16], [17].

MLE is one of the most widely adopted approaches to PGO. Under the circumstances typically encountered in robotics and computer vision applications, the isotropic Gaussian and Langevin [18] noise models adopted therein provide an accurate description of real-world phenomena. That being the case, what may be gained in accuracy through this approach, gives way to reduced tractability due to the non-convexity of the problem, associated with $SO(p)$. In fact, unrestricted retrieval of optimal solutions in this group is only possible for cycle graphs [14], [19].

For this reason, earlier works all shared one common ground: that of being local search methods, with no optimality guarantees. Such was the case of Gauss-Newton based-techniques, as the ones implemented in the popular frameworks g2o [3] and GTSAM [4]. These initialization-dependent iterative approaches, ultimately led to a large body of works concerning *good initializations* i.e., initial pose guesses from where the aforementioned methods are expected to attain the optimum. These initializations, often heuristic in nature, solve a simpler proxy problem in $SO(p)$ and may be iterative themselves e.g., the graph consensus formulation by Tron et al. [8] which is solved on the $SO(p)$ manifold directly using the Riemannian gradient. Alternatively, the closed-form spectral initialization featured in [6], [10], [13], which involves the projection of the p eigenvectors of the connection Laplacian corresponding to the smallest eigenvalues, yields a good approximation of the optimum for moderate noise levels. This approximation is well understood at this point, with suboptimality bounds given for $SO(2)$ [6] and $SO(3)$ [20]. In addition, it lends itself to high-performance implementations by leveraging the sparsity of the graph [21]. For a more complete survey and benchmark of PGO initializations, see Carlone et al. [1].

While the combination of Gauss-Newton with an appropriate initialization makes for a good strategy to avoid suboptimal accumulation points, the issue of optimality verification

persists. This was ultimately overcome via duality theory. While, as we mentioned, problem (1) is non-convex, its dual and bi-dual are SDPs which can be solved in polynomial time via interior-point methods, the latter being the convex relaxation of (1). This convexification of the problem has been the go-to strategy in recent research since it provides either an optimality certificate or a means to ascertain how suboptimal a given solution is. Eriksson et al. [9] derived the dual and bi-dual SDP of the problem in $SO(p)$ i.e., rotation averaging, and solve the latter using a block-coordinate descent approach. Carlone et al. [2] also rely on the dual to solve the primal in $SE(3)$. For phase synchronization in the complex circle group, Boumal [6] proposed the Generalized Power Method, which is an application of the Frank-Wolfe method, achieving linear convergence [22].

Apart from the non-convexity, the second difficulty inherent to PGO is the high-dimensionality of the problem. If on the one hand the bi-dual SDP allow us to bypass PGO's non-convex nature, on the other hand, the new problem involves a $np \times np$ dense matrix variable, which in common applications can easily reach upwards of 10^8 entries. To address this issue, Rosen et al. [13] leveraged the results of Burer-Monteiro [23] on the low-rank solutions of SDPs and proposed a Riemannian staircase [11] to solve the SDP via increasing rank factorizations. In the same paper, the authors also derive bounds for the tightness of the convex relaxation i.e., the duality gap, as a function of the graph connectivity and the degradation level of the measurements. This effectively proved that in well connected graphs there is greater leeway in how degraded the pairwise measurements can be, before solutions are no longer certifiable. This low-rank approach to the SDP was also featured in Shonan averaging [24], wherein the rank increase is realized by searching over $SO(q)$ for $q \geq p$.

4 PROBLEM STATEMENT

We start by the noise model commonly adopted in the literature and the nonconvex MLE problem derived upon it. We then set forth the Lagrangian and the SDP dual problem.

Consider a set of n vertices $\mathcal{V} = \{1, \dots, n\}$. We parameterize each vertex with a latent position $t_i \in \mathbb{R}^p$ and a latent orientation $R_i \in SO(p)$. In other words, each vertex $i \in \mathcal{V}$ is associated with a pose $x_i \in SE(p)$ i.e., a rigid (Euclidean) transformation (R_i, t_i) . For every pairwise tuple $(i, j) \in \mathcal{V}^2$, we define relative transformations as $x_{ij} := x_i x_j^{-1}$. It follows that $R_{ij} := R_i R_j^T$ encodes the latent relative orientation of vertex i w.r.t. vertex j and $t_{ij} = t_i - R_i^T t_j$ the position of the i -th vertex as seen from the reference frame of vertex j . The input to a PGO problem is a set of noisy relative pose measurements $\{(\tilde{R}_{ij}, \tilde{t}_{ij})\}$, for $(i, j) \in \mathcal{E} \subseteq \mathcal{V}^2$. The goal is to estimate the n latent poses $\{(R_i, t_i)\}_{i \in \mathcal{V}}$ that originated those relative measurements.

We assume that G is connected. This hypothesis is necessary due to an inherent ambiguity of this estimation problem. Without anchoring any of the vertices, the set of poses $\{(R_i, t_i)\}_{i \in \mathcal{V}}$ is equivalent to $\{R_i \hat{R}, R_i \hat{t} + t_i\}_{i \in \mathcal{V}}$ for any rigid transformation (\hat{R}, \hat{t}) . This is known as gauge freedom. In Fig. 1 e.g., we can globally rotate and translate the entire

mesh, without affecting the relative poses of the vertices. If the underlying graph is not connected, the disconnected components may each be independently optimized up to a rigid transformation, but never with respect to a common reference frame, which is undesirable. We also assume that the graph G is cyclic, i.e., it has at least one cycle, since it is the existence of cycles that leads to inconsistencies and thus to an optimization problem. In the absence of cycles, the only possible pose estimates are given by the composition of relative transformations along paths originating in a common vertex.

4.1 MLE formulation of PGO

The model most commonly adopted in the literature consists of additive isotropic white Gaussian noise for the translation variables

$$\tilde{t}_{ij} = t_{ij} + e_{ij} = t_i - \underline{R}_j^\top t_j + e_{ij}, \quad (11)$$

where $e_{ij} \sim \mathcal{N}(0, \tau_{ij}^{-1} I_d)$ with pdf

$$F_{\text{Gaussian}}(e; 0, \tau^{-1} I_d) \propto \exp\left(-\frac{\tau}{2} \|e\|_2^2\right) \quad (12)$$

and isotropic Langevin noise for the rotations

$$\tilde{R}_{ij} = \underline{R}_{ij} R_{ij}^\epsilon = \underline{R}_i \underline{R}_j^\top R_{ij}^\epsilon, \quad (13)$$

where $R_{ij}^\epsilon \sim \text{Langevin}(I_p, \kappa_{ij})$, with κ_{ij} being the concentration parameter with the Langevin pdf [25]

$$F_{\text{Lang}}(R^\epsilon; I_p, \kappa) \propto \exp(\kappa \text{tr}(R^\epsilon)). \quad (14)$$

Under the assumption of measurement independence, the log-likelihood function reads as

$$f_{\text{ML}} = \sum_{i \sim j} \kappa_{ij} \|R_i - \tilde{R}_{ij} R_j\|_F^2 - \tau_{ij} \|\tilde{t}_{ij} - t_i + \underline{R}_j^\top t_j\|_2^2. \quad (15)$$

The log-likelihood f_{ML} is non-concave. However, it is concave in the translation variables. In [13], the authors showed that maximizing the log-likelihood is equivalent to solving first a rotation-only synchronization problem and then computing the optimal translations, which is a least-squares problem. We can thus focus our attention on the problem of finding the optimal rotations. Let the connection adjacency $\tilde{A} \in \mathbb{R}^{np \times np}$ for the rotational problem be defined as the symmetric $p \times p$ -block matrix

$$\tilde{A}_{ij} := \begin{cases} \kappa_{ij} \tilde{R}_{ij}, & (i, j) \in E \\ 0_{p \times p}, & \text{otherwise.} \end{cases} \quad (16)$$

Letting $d_i := \sum_{i \sim j} \kappa_{ij}$ and $D \in \mathbb{R}^{np \times np}$ the block diagonal

$$D := \text{Diag}(d_1 I_p, \dots, d_n I_p), \quad (17)$$

we have the connection Laplacian given by $\tilde{L} := D - \tilde{A}$. Stacking the rotation matrices horizontally in a column block-vector $R \in \text{SO}(p)^n \subset \mathbb{R}^{np \times p}$

$$R := [R_1^\top \quad \dots \quad R_n^\top]^\top, \quad (18)$$

the rotation synchronization problem can be stated as the minimization of a quadratic in $\text{SO}(p)^n$,

$$\begin{aligned} & \underset{R}{\text{minimize}} && -\langle RR^\top, \tilde{A} - \tilde{Q}^\tau \rangle \\ & \text{subject to} && R \in \text{SO}(p)^n, \end{aligned} \quad (19)$$

where \tilde{Q}^τ is a dense matrix containing the translation terms [13]. If we only retain the \tilde{A} term, we obtain the rotation averaging problem [5], [9], [24]

$$\begin{aligned} & \underset{R}{\text{minimize}} && -\langle RR^\top, \tilde{A} \rangle \\ & \text{subject to} && R \in \text{SO}(p)^n. \end{aligned} \quad (20)$$

Problems (19) and (20) are both instances of the orthogonal-cut problem. The former providing the solution for measurements in $\text{SE}(p)$ and the latter used either as a rotation-only initialization for the former or as a standalone problem for measurements in $\text{SO}(p)$, with applications such as clock synchronization in $\text{SO}(2)$ and structure-from-motion in $\text{SO}(3)$. In what follows, we will focus on the Rotation Averaging Problem (20), considering the concentration parameters κ_{ij} to be identically 1.

4.2 From non-convex MLE to strong duality

We shall now briefly summarize the theory underlying optimality certification for Problem (20). We refer the reader to [9], [13] for the detailed proofs. Let $\Lambda := \text{Diag}(\Lambda_1, \dots, \Lambda_n)$ be a symmetric $p \times p$ -block diagonal dual variable. The Lagrangian of Problem (20) is

$$\mathcal{L}(R, \Lambda) = -\langle R, \tilde{A}R \rangle - \langle \Lambda, (RR^\top - I_{np}) \rangle. \quad (21)$$

Differentiating \mathcal{L} w.r.t. R , we have the first-order KKT condition

$$\tilde{A}R = \Lambda R, \quad (22)$$

which allows us to retrieve Λ from $\tilde{A}R$ as $\Lambda_i = \sum_j \tilde{A}_{ij} R_j R_i^\top$ and conversely, R from the kernel of $\Lambda - \tilde{A}$. The dual of Problem (20) is the SDP

$$\begin{aligned} & \underset{\Lambda}{\text{maximize}} && -\text{tr}(\Lambda) \\ & \text{subject to} && \Lambda - \tilde{A} \succeq 0. \end{aligned} \quad (23)$$

From duality theory [9], [13], if $\exists R, \Lambda$ feasible such that (22) holds, then $\Lambda - \tilde{A} \succeq 0$, is enough to guarantee that the pair (R, Λ) is primal-dual optimal i.e., the duality gap between the primal (20) and the dual (23) is zero. The matrix $\Lambda - \tilde{A}$ provides thus an optimality certificate, provided it is positive-semidefinite. In fact, let $\lambda_1 \leq \dots \leq \lambda_{np}$ be the eigenvalues of $\Lambda - \tilde{A}$. Then, for R, Λ primal-dual feasible, the duality gap is bounded below as

$$-\langle R, \tilde{A}R \rangle + \text{tr}(\Lambda) \geq np(\lambda_1 + \lambda_2 + \lambda_3). \quad (24)$$

For connected graphs, the latent connection Laplacian defined as $\underline{L} := D - \underline{A}$ is both positive semidefinite and has nullity of p . Thus, not only is D the best candidate for the optimal Λ^* , but in this case the optimum R^* , which is equal to its latent counterpart \underline{R} , actually lies in the kernel of the \underline{L} . Evidently, in the real world the latent connection Laplacian is unknown. In addition, the real connection Laplacian $\tilde{L} = D - \tilde{A}$ no longer has a kernel. Nevertheless, D which is known from the graph topology (the graph degree matrix), is still dual-feasible and may be a good approximation of Λ^* . The suboptimality of this estimate is, according to (24), bounded by the smallest eigenvalues of $\tilde{L} = D - \tilde{A}$. This is the crux of the spectral initialization, which takes the eigenspace spanned by the p eigenvectors of \tilde{L} corresponding to the smallest eigenvalues, and projects

them orthogonally to $\text{SO}(p)^n$. As we shall expound in the subsequent section, the proposed primal-dual method exploits this further by starting with $\Lambda_{(0)} = D$ and iteratively updating the dual estimate.

5 PRIMAL-DUAL METHOD

In this section, we present a primal-dual method to solve Problem (20). The building blocks to arrive at a primal-dual method are the first-order KKT condition (22) of the problem and the Generalized Power Method (GPM) proposed in [6]. The former will be used to compute primal updates $R_{(k)}$, in a similar fashion to the spectral initialization. The latter is used to produce the dual estimates $\Lambda_{(k)}$.

5.1 Primal update

Given an estimate of the dual variable e.g., D , the KKT condition (22) will in general not have a solution in $\text{SO}(p)^n$. The spectral initialization resorts thus to an approximation, by first relaxing the orthogonality constraint $\text{BlockDiag}(XX^\top) = I_{np}$ for $X^\top X = nI_p$, i.e. it supplants orthogonality of the $p \times p$ blocks of X for column orthogonality. The relaxation thereby obtained

$$\arg \min_{X^\top X = nI_p} \langle XX^\top, (D - \tilde{A}) \rangle, \quad (25)$$

can be solved by computing the eigenvectors of $D - \tilde{A}$ corresponding to the smallest eigenvalues. These eigenvectors are then projected to $\text{SO}(p)^n$ via an orthogonal projection, to obtain the feasible primal estimate, denoted by $R_{(0)}$.

The focal point of our update rule lies in starting with the spectral initialization i.e., $\Lambda_{(0)} = D$, but updating this block diagonal matrix afterwards with a better, yet infeasible, dual estimate $\Lambda_{(k)}$. For the primal update, given $\Lambda_{(k)}$ at the k -th iteration, we solve thus

$$X_{(k+1)} = \arg \min_{X^\top X = nI_p} \langle XX^\top, (\Lambda_{(k)} - \tilde{A}) \rangle \quad (26)$$

$$R_{(k+1)} = \arg \min_{R \in \text{SO}(p)^n} \|R - X_{(k+1)}\|_F^2. \quad (27)$$

The gauge-invariant distance from this estimate to the global optimum R^* of Problem (20), which we write as

$$d_{(0)} := \min_{G \in \text{SO}(p)} \|R^* - R_{(0)}G\|_F, \quad (28)$$

was bounded by Doherty et al. [20] for $k = 0$ as

$$d_{(0)} \leq \frac{(8 + 4\sqrt{2})\sqrt{np}\|\tilde{A} - \underline{A}\|_2}{\lambda_{p+1}(\underline{L})}, \quad (29)$$

wherein we witness the influence of the noise in $\|\tilde{A} - \underline{A}\|_2$ and the inverse relationship with the connectivity of the graph, indicated by its Fiedler value $\lambda_{p+1}(\underline{L})$. In our case, the bound in (29) becomes

$$d_{(k)} \leq (8 + 4\sqrt{2})\sqrt{np} \frac{\|(\Lambda_{(k)} - D) - (\tilde{A} - \underline{A})\|_2}{\lambda_{p+1}(\underline{L})}. \quad (30)$$

Similarly to the spectral initialization, the solution of (26) can be computed efficiently by means of sparse Krylov-based symmetric eigensolvers, as in [21]. The optimization

problem in (27) can be solved via n SVDs of $p \times p$ matrices. Further, given a primal-dual pair (R^*, Λ^*) that verifies the stationarity condition (22), $\Lambda^* - \tilde{A} \succeq 0$ provides an optimality certificate. Thus, (26) allows for an optimality assessment at each iteration.

5.2 Dual update

In order to formulate the dual update, we start by recalling the recursion of GPM. Define the orthogonal projection from $\mathbb{R}^{np \times p}$ to $\text{SO}(p)^n \subset \mathbb{R}^{np \times p}$ as the map

$$P(X) = \arg \min_{R \in \text{SO}(p)^n} \|X - R\|_F^2, \quad (31)$$

which has a closed-form solution given by the blockwise SVD of X . GPM is realized via fixed-point iterations of the operator P i.e.,

$$R_{(k+1)} = P(\tilde{A}R_{(k)}). \quad (32)$$

As noted by the authors, this is an application of the Frank-Wolfe method since $\tilde{A}R_{(k)}$ is the linearization of the quadratic in Problem (20). Alternatively, it may also be viewed as a projected gradient method. Convergence of (32) is shown to be linear in $\text{SO}(2)$ [22].

We will now write the fixed-point iterations (32) in terms of the dual variable, thus reformulating GPM itself as an infeasible primal-dual method. Compute the SVD of the i -th block $(\tilde{A}R_{(k)})_i$ as $U_i \Sigma_i V_i^\top$ and set

$$\Lambda_{(k)} = \text{Diag}(U_1 \Sigma_1 U_1^\top, \dots, U_n \Sigma_n U_n^\top). \quad (33)$$

Then, the GPM update may be written as

$$R_{(k+1)} = \Lambda_{(k)}^{-1} \tilde{A}R_{(k)}. \quad (34)$$

If $R_{(\infty)}$ and $\Lambda_{(\infty)}$ are accumulation points of the sequence defined in (34) then, $R_{(\infty)} = \Lambda_{(\infty)}^{-1} \tilde{A}R_{(\infty)}$, which is the KKT condition (22) of the primal problem. Further, similarly to the monotonous increase in $\langle R_{(k)}, \tilde{A}R_{(k)} \rangle$, we have for $\Lambda_{(k)}$ the following result.

Lemma 1. *The dual iterates $\Lambda_{(k)}$ of GPM defined by the recursion (34) verify $\text{tr}(\Lambda_{(k+1)}) \geq \text{tr}(\Lambda_{(k)})$ (proof in the appendix).*

Note that, in spite of this reformulation of GPM as a primal-dual method, the iterates $\Lambda_{(k)}$ are not dual-feasible.

Lemma 2. *Assume $\tilde{A} \succeq 0$. The updates defined by the recursion (34) are dual infeasible (proof in the appendix).*

To form the dual update, we rely on the reformulation of GPM just presented, in particular the recursion in (34). Given a primal estimate $R_{(k)}$, we compute an iteration of GPM as

$$\tilde{A}R_{(k)} = \Lambda_{(k)}Y. \quad (35)$$

Here, $Y \in \text{SO}(p)^n \subset \mathbb{R}^{np \times p}$ would be the next primal estimate in the GPM sequence. However, we only retain the dual estimate $\Lambda_{(k)}$. In more explicit notation, from the SVDs

$$\sum_{j \in \delta_i} \tilde{A}_{ij} R_{(k)_j} = U_i \Sigma_i V_i^\top, \quad i = 1, \dots, n \quad (36)$$

we set $\Lambda_{(k)_i} = U_i \Sigma_i U_i^\top$. Note that this approach is comparable to the work of Gao et al. [26] on optimization problems

with orthogonality constraints, wherein the dual update is achieved by symmetrizing $\sum_{j \in \delta_i} \tilde{A}_{ij} R_{(k)_j} R_{(k)_i}^\top$ i.e.,

$$\Lambda_{(k)_i} = \frac{1}{2} \sum_{j \in \delta_i} \tilde{A}_{ij} R_{(k)_j} R_i^\top + \frac{1}{2} \left(\sum_{j \in \delta_i} \tilde{A}_{ij} R_{(k)_j} R_i^\top \right)^\top \quad (37)$$

In Algorithm 1 we show how our primal-dual updates were implemented. The parameter σ used in the sparse eigensolver corresponds to the eigenvalue target for the eigenvectors we are computing. Since our primal update is achieved by solving (26), we pick $\sigma < 0$ such that the three eigenvectors retrieved correspond to the three smallest eigenvalues. Prior to projecting the solution of the primal problem we fix the gauge freedom by anchoring the first rotation, chosen arbitrarily.

Algorithm 1: Primal-Dual in SO(p)

```

input :  $\tilde{A}, D$  // Adjacency and degree
output:  $R, \Lambda$ 
 $\Lambda \leftarrow D$ 
for  $t \leftarrow 0$  to  $\maxiter$  do
     $X, \lambda_1, \dots, \lambda_p \leftarrow \text{eigensolver}(\Lambda - \tilde{A})$ 
     $X \leftarrow X X_1^{-1}$  // Gauge fix
    for  $i \leftarrow 2$  to  $n$  do
         $U \Sigma V^\top \leftarrow \text{SVD}(X_i)$ 
         $R_i \leftarrow U \text{diag}([1 \ 1 \ \dots \ \det(UV^\top)]) V^\top$ 
    end
     $Y \leftarrow \tilde{A} R$ 
    for  $i \leftarrow 1$  to  $n$  do
         $U_i \Sigma_i V_i^\top \leftarrow \text{SVD}(Y_i)$ 
         $\Lambda_i \leftarrow U_i \Sigma_i U_i^\top$ 
    end
     $\Lambda \leftarrow \text{BlockDiag}(\Lambda_1, \dots, \Lambda_n)$ ;
    if  $\min\{|\lambda_1|, \dots, |\lambda_p|\} < \epsilon$  then
        return  $R, \Lambda$ 
    end
end
    
```

We conclude this section by noting that the primal-dual iterations can easily be adapted to the problem of angular synchronization, by using the complex circle group $S = \{z \in \mathbb{C} \mid |z| = 1\}$ to represent rotations, instead of the matrix group SO(2). In this case, $\tilde{A} \in \mathbb{C}^{n \times n}$ is Hermitian, with $\tilde{A}_{ij} = \tilde{z}_{ij}$ for $(i, j) \in \mathcal{E}$. In the spectral step of the primal update, only one eigenvector is computed, corresponding to the smallest eigenvalue. This eigenvector is element-wise projected to S via $z_i \leftarrow z_i / |z_i|$. For the dual update, Λ is a real $n \times n$ diagonal matrix. Instead of the SVD, Λ_i is updated to the magnitude of $\sum_{j \in \delta_i} \tilde{z}_{ij} z_j$.

6 CYCLE GRAPHS

From a topological standpoint, cycle graphs are the simplest instance of rotation averaging. Implementation-wise, they are the ones where sparsity may be exploited the most. From a theoretical viewpoint, closed-form solutions for the global optima are known [19]. A natural consequence of this is that they present an adequate benchmark for iterative methods [9], [24]. In this section, we characterize the solutions of the stationary points for rotation averaging problems with an

underlying cycle graph topology, global optima included. We do so in via a different approach than the one adopted in [19]. We will first derive the closed-form solutions for one-parameter subgroups of SO(3). We then show that, in the general case, there is a basis wherein the connection adjacency matrix \tilde{A} can be written such that the measurements lie in a one-parameter subgroup of SO(3). These results culminate in the proof that the primal-dual iterations (Algorithm 1) retrieve the global optimum in cycle graphs, after one iteration.

We start by defining the error $E \in \text{SO}(3)$ incurred while traversing the cycle graph starting and ending on the same node. Without loss of generality let

$$E := \prod_{k=0}^{n-1} \tilde{R}_{\text{mod}(k,n)+1, \text{mod}(k+1,n)+1}, \quad (38)$$

with the matrix product in (38) being defined from left to right. In a cycle with 3 nodes e.g., $E = \tilde{R}_{12} \tilde{R}_{23} \tilde{R}_{31}$.

Further, let $\gamma \in [-\pi, \pi]$ be the angle of E , which we denote by $\gamma := \angle(E)$. We define the set of the n -th roots of E as

$$E^{\frac{1}{n}} := \{E_0, E_1, \dots, E_{n-1}\}, \quad (39)$$

with $E_k \in \text{SO}(3)$, $E_k^n = E$ and $\angle(E_k) = \gamma/n - 2k\pi/n$, for $k \in \{0, \dots, n-1\}$.

6.1 One-parameter subgroups of SO(3)

We consider for now one-parameter subgroups of SO(3) by assuming that the pairwise rotation measurements $\tilde{R}_{12}, \tilde{R}_{23}, \dots, \tilde{R}_{n1}$ share a common axis. We start by characterizing its stationary points.

Lemma 3. *For cycle graphs whose edge measurements lie in a one-parameter subgroup of SO(3), the points*

$$R_i = \left(\prod_{s=1}^{i-1} \tilde{R}_{s,s+1} \right)^\top E_k^{i-1}, \quad i \in \{2, \dots, n\} \quad (40)$$

with $R_1 = I_3$, indexed by $k \in \{0, \dots, n-1\}$, are stationary points of problem (20).

From Lemma 3, we arrive at the optimal solution in SO(2) in the following result.

Theorem 4. *For cycle graphs whose edge measurements lie in a one-parameter subgroup of SO(3), the point*

$$R_i^* = \left(\prod_{k=1}^{i-1} \tilde{R}_{k,k+1} \right)^\top E_0^{i-1}, \quad i \in \{2, \dots, n\} \quad (41)$$

with $R_1^* = I_3$ is a solution of problem (20).

Proof. Invoking Theorem 4.2 of [9] for cycle graphs, strong duality will hold and a solution will be globally optimal if $\forall i \sim j$ the residuals verify $|\theta_{ij} - \theta_{ij}^*| \leq \frac{\pi}{n}$. From (41), the optimal rotations verify

$$R_j^* = E_0 \tilde{R}_{ij}^\top R_i^*, \quad (42)$$

with $\angle(E_0) = \gamma/n$. From (42) we can write

$$\tilde{\theta}_{ij} - \theta_{ij}^* = \angle(\tilde{R}_{ij} R_j^* R_i^{*\top}) = \gamma/n, \quad (43)$$

Since

$$|\gamma/n| \leq \frac{\pi}{n} \quad (44)$$

due to $\gamma \in [-\pi, \pi]$, the solution in (41) is optimal. \square

In cycle graphs, rotation averaging problems in one-parameter subgroups of $\text{SO}(3)$ will redistribute the cycle error equitably over all of the edges. If we incur a cycle error of E , with $\angle(E) = \gamma$, the optimal relative rotation $R_i^* R_j^{*\top}$ will have an angular residual of γ/n relative to the respective measurement \tilde{R}_{ij} . By increasing this figure by a multiple of $2\pi/n$ we obtain suboptimal stationary points of Problem (20). Borrowing the spring system analogy of Section 1, in stationary points the net force at each vertex will be zero. In a cycle, this can only happen if the spring displacements i.e., the residuals, are the same everywhere.

6.2 Optimization in $\text{SO}(3)$

We now show that any cycle graph problem in $\text{SO}(3)$ has the same expression for its stationary points (40) and global optimum (41) as derived for one-parameter subgroups. We accomplish this by rewriting \tilde{A} in a new basis.

Define the matrix $U \in \text{SO}(3n)$ as

$$U := \text{BlockDiag}(U_1, \dots, U_n), \quad (45)$$

with $U_i \in \text{SO}(3)$ for $i \in \{1, \dots, n\}$ computed according to

$$U_i := \begin{cases} I_3, & i = 1 \\ \tilde{R}_{i-1,i}^\top U_{i-1}, & i \in \{2, \dots, n\}. \end{cases} \quad (46)$$

Denote by \tilde{A}' , the matrix \tilde{A} written in the basis U i.e., $\tilde{A}' := U^\top \tilde{A} U$. From (46), the blocks on the lower triangular part of $\tilde{A}' := U^\top \tilde{A} U$ are given by

$$\tilde{A}'_{ij} = \begin{cases} U_n^\top \tilde{R}_{n1} U_1, & i = n, j = 1 \\ U_i^\top \tilde{R}_{ij} \tilde{R}_{ij}^\top U_i, & j = i - 1 \\ 0_{3 \times 3}, & i = j. \end{cases} \quad (47)$$

It is immediate that for $j = i - 1$ we have $\tilde{R}'_{ij} = I_3$. It suffices to show that $U_n^\top \tilde{R}_{n1} U_1 = E$. Note that from (46) we have $U_1 = I_3$ and $U_n = \tilde{R}_{n-1,n}^\top \dots \tilde{R}_{23}^\top \tilde{R}_{12}^\top$. Therefore,

$$U_n^\top \tilde{R}_{n1} U_1 = \tilde{R}_{12} \tilde{R}_{23} \dots \tilde{R}_{n-1,n} \tilde{R}_{n1}, \quad (48)$$

which equals E i.e., the cycle error (38), by definition of the latter. Thus,

$$\tilde{A}' = \begin{bmatrix} 0_{3 \times 3} & I_3 & \dots & 0 & E^\top \\ I_3 & 0_{3 \times 3} & \dots & 0 & 0 \\ \vdots & \vdots & \ddots & \vdots & \vdots \\ 0 & 0 & \dots & 0_{3 \times 3} & I_3 \\ E & 0 & \dots & I_3 & 0_{3 \times 3} \end{bmatrix} \quad (49)$$

We can visualize this result in Fig. 3. In cycle graphs, MLE rotation averaging can be solved by concentrating the cycle error E at a single edge. Further, by changing basis, the pairwise measurements I_p and E belong to a one-parameter subgroup of $\text{SO}(3)$. We can thus leverage the results from Section 6.1 to retrieve the global optimum and stationary points of problem in closed-form.

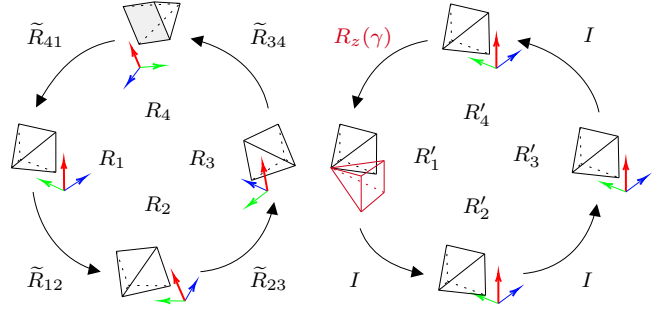


Fig. 3. The cycle graph problem on the left can be transformed into the problem on the right via a change-of-basis.

Theorem 5. For cycle graphs with edge measurements in $\text{SO}(3)$, the point

$$R_i^* = \left(\prod_{s=1}^{i-1} \tilde{R}_{s,s+1} \right)^\top E_0^{i-1}, \quad i \in \{2, \dots, n\} \quad (50)$$

with $R_1^* = I_3$, is a solution of the problem (20).

Proof. We rewrite the cost function as as

$$f(R) = \langle (U^\top R, U^\top \tilde{A} U (U^\top R)) \rangle. \quad (51)$$

Using the change-of-variables $R' = U^\top R$ and the change-of-basis $\tilde{A}' = U^\top \tilde{A} U$ we have the equivalent problem

$$\begin{aligned} & \text{minimize}_{R'} \quad \langle R', \tilde{A}' R' \rangle \\ & \text{subject to} \quad R' \in \text{SO}(3)^n, \end{aligned} \quad (52)$$

whose edge measurements either I_p or E . These rotations belong to the one-parameter subgroup $t \mapsto \exp(t[\hat{n}]_\times)$, where \hat{n} is the axis of E . Theorem 4 is thus applicable and the solution of (52) is

$$R'_i = E_0^{i-1}, \quad i \in \{1, \dots, n\}, \quad (53)$$

since $\tilde{R}'_{i,i+1} = I_3, \forall i \in \{1, \dots, n-1\}$. It suffices now to write (53) in the old basis vectors according to $R^* = U R'^*$. Since U is block-diagonal, $R_i^* = U_i R'_i$. From the definition of U_i (46) we have

$$R_i^* = \left(\prod_{s=1}^{i-1} \tilde{R}_{s,s+1} \right)^\top E_0^{i-1}, \quad i \in \{2, \dots, n\} \quad (54)$$

with $R_1^* = I_3$. \square

As a corollary of Theorem 5, we can take any stationary point of the problem in the new basis (see Lemma 3) and revert to the old basis vectors in order to obtain the corresponding stationary point of problem. Thus, the points

$$R_i = \left(\prod_{s=1}^{i-1} \tilde{R}_{s,s+1} \right)^\top E_k^{i-1}, \quad i \in \{2, \dots, n\} \quad (55)$$

with $R_1 = I_3$, are stationary points of (20) indexed by $k \in \{0, \dots, n-1\}$, where the cost function evaluates to

$$f(R) = -2n \text{tr}(E_k). \quad (56)$$

Since $\text{tr}(E_k) = 1 + 2 \cos(\gamma/n - 2k\pi/n)$ it follows that the greater the number of nodes, the greater the number of local

minima near the global optimum. Hence the difficulty of solving rotation averaging optimally.

Further, in cycle graphs the spectrum of \tilde{A} relates to the values of the cost function at stationary points and can therefore be computed in closed-form.

Theorem 6. Let $\sigma(\tilde{A})$ denote the spectrum of \tilde{A} . Then,

$$\begin{aligned} \sigma(\tilde{A}) = & \{2 \cos(\gamma/n - 2k\pi/n)\}_{k=0, \dots, n-1} \\ & \cup \{2 \cos(2k\pi/n)\}_{k=0, \dots, n-1} \end{aligned} \quad (57)$$

(proof in the appendix).

We conclude this section by showing that, for cycle graphs the primal-dual method (Algorithm 1) retrieves the rotation averaging global optimum in $SO(3)$ at the first iteration. Letting $\Lambda_{(0)} = D$, from the proof of Theorem 6, we know that the equation for the eigenvectors of \tilde{A}' corresponding to the three largest eigenvalues is

$$\tilde{A}' \begin{bmatrix} I \\ E \\ E^2 \\ \vdots \\ E^{n-1} \end{bmatrix} J = \begin{bmatrix} I \\ E \\ E^2 \\ \vdots \\ E^{n-1} \end{bmatrix} J \Sigma. \quad (58)$$

Changing bases, $\tilde{A}' = U^\top \tilde{A} U$ and attending to the definition of U (45) yields

$$\tilde{A} R^* J = R^* J \Sigma. \quad (59)$$

Thus, the first spectral update of the primal-dual method satisfies the equation

$$(\Lambda_{(0)} - \tilde{A}) R^* J = R^* J (2I_3 - \Sigma). \quad (60)$$

Since $R^* J \in SO(3)^n$, the orthogonal projection is the identity. The dual update is then given via the blockwise SVD of $\tilde{A} R^* J$ i.e.,

$$\Lambda_{(1)} = \text{BlockDiag}(R_1^* J \Sigma J^\top R_1^{*\top}, \dots, R_n^* J \Sigma J^\top R_n^{*\top}) \quad (61)$$

which verifies $(\Lambda_{(1)} - \tilde{A}) R^* = 0$.

7 EXPERIMENTAL RESULTS

In this section, we evaluate the performance of our primal-dual method and our closed-form solution in pose graph datasets and synthetic rotation averaging problems in cycle graphs, respectively. Our algorithms were implemented in C++ and all the tests were conducted on a laptop computer with a 6-core Intel Core i7-9750H@2.6GHz.

7.1 Optimality

In order to analyze the conditions under which the primal-dual iterations proposed succeeded in retrieving the global optimum, we will invoke one key result from [13], Proposition 2 on the exact recovery of the solution via the SDP relaxation. This proposition states that $\exists \beta > 0$, function of the ground-truth connection Laplacian \underline{L} such that if $\|\tilde{L} - \underline{L}\|_2 < \beta$, the duality gap is zero. This spectral norm is an indication of how degraded the measurements are. Since we expect β to depend on the graph connectivity, in Fig. 4 we plot the frequency of optimal solution retrieval for

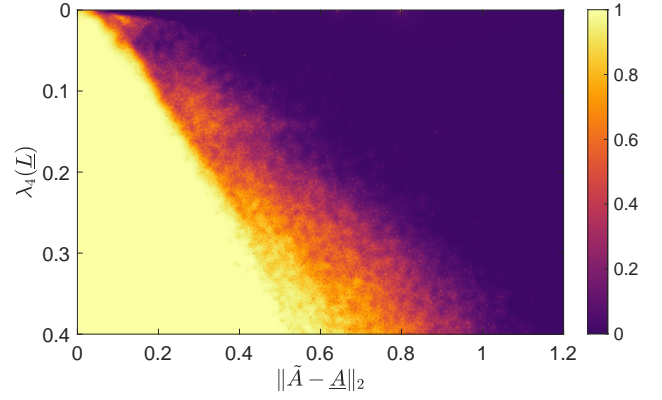


Fig. 4. Primal-dual convergence to the optimum in $SO(3)$ (color represents frequency). Vertical axis: Graph's Fiedler value (same as the 4th eigenvalue of the latent connection Laplacian \underline{L}). Horizontal axis: operator norm of the difference between the latent and measured connection adjacency matrices, \underline{A} and \tilde{A} , respectively. Axes in multiples of n .

10^5 combinations of the underlying graph's Fiedler value (vertical axis) and the aforementioned spectral norm (horizontal axis). By inspecting the plot, we can see that for larger graph connectivities, a larger maximum noise threshold below which certifiable optimal recovery is possible. The relationship between the two is approximately linear.

7.2 Cycle graphs

Borrowing the evaluation approach adopted in [9], [24], we tested our primal-dual algorithm, in synthetic cycle graph datasets. These consisted of random rotation averaging problems with underlying cycle graph structures of different sizes, wherein the ground-truth absolute orientations R_i correspond to rotations around the z-axis, forming a circular trajectory. The synthetic pairwise measurements were simulated by perturbing the relative ground-truth orientations between adjacent nodes by an error matrix obtained from angle-axis representations. The axes were sampled uniformly over the unit sphere. The angles were drawn from a normal distribution with zero mean and standard deviation σ .

We benchmarked our method against two baselines, the block coordinate descent method (BCD) [9] used to solve the bi-dual of problem (20) and the SA algorithm which we also tested in our pose graph experiments. We implemented the former in MATLAB and used the author's implementation of the latter. Both methods were initialized randomly. Results averaged over 20 simulations can be observed in Table 2. For our solution, we list the average of the smallest eigenvalue of $\Lambda^* - \tilde{A}$, denoted by $|\bar{\lambda}_1|$, which certifies that, as we have shown, our solution is optimal to machine precision in all the simulations we ran. In the two rightmost columns, we show the average difference $\bar{\Delta}^*$ between our closed-form global minimum and the cost function evaluated at the set of rotations produced by SA and BCD.

Using its default settings, SA retrieved the global optimum in all the tests conducted. Nevertheless, not only does precision wane as the order of the cycle increases but also the average CPU time surges substantially as the number

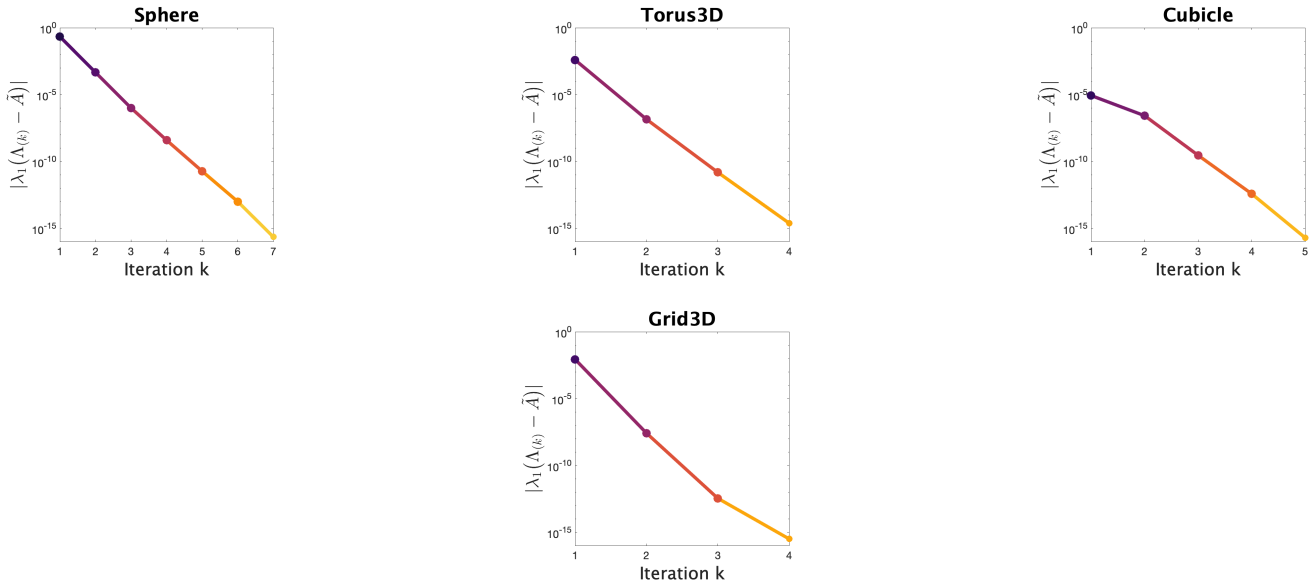


Fig. 5. Convergence of absolute value of the smallest eigenvalue of $\Lambda_{(k)} - \tilde{A}$ for the PGO datasets Sphere (0.36s), Torus3D (0.35s), Cubicle (0.46s) and Grid3D (1.78s), made available in [1], [2].



Fig. 6. Cycle graph 3D reconstruction with 38 poses. Rotation averaging using the primal-dual algorithm (1) takes 2ms. For reference, our implementation of the closed-form solution takes 0.07ms.

of variables increases. In order to test the BCD method, we first computed the global optimum in each simulation via the closed-form solution. We then used it to set the stopping criterion for the BCD as $\Delta^* \leq 10^{-3}$. As evidenced by the average CPU time, convergence flatlined for the largest cycles. Attaining the global minimum to three decimal places using this algorithm took, on average, as much as 96 seconds for $n = 100$ and longer than that would be required for $n = 200$. While this may be a shortcoming of our implementation, the orders of magnitude of the CPU time appear to be in accordance with those reported in [24].

7.3 PGO benchmarks

Using seven datasets from the pose graph optimization literature available online [1], we extracted the pairwise rotation measurements from each one in order to generate rotation averaging problems. Some of these datasets contain multiple measurements per edge, from which only one was kept. We compare the performance the primal-dual method in Algorithm 1) against Shonan Averaging (SA) [24] and SE-Sync [13]. The authors’ implementations are available online and we tested them with their default parameters. Since SE-Sync is designed for solving pose graph optimization

problems, we set the input translations to zero. The stopping criterion for our method was defined as $|\lambda_1| < 10^{-15}$, which corresponds to tolerance of the Krylov-based eigensolver used.

The results can be observed in Table 1. In order to juxtapose the three methods in terms of the positive semidefiniteness of $\Lambda - \tilde{A}$ i.e., in order to verify optimality, we proceeded as follows. For each estimate computed, we obtained the Lagrange multiplier using the KKT condition in (22) and symmetrized it. The columns λ_1 in Table 1 correspond to the minimum eigenvalue of $\Lambda - \tilde{A}$, which is zero if a given solution is optimal and strong duality holds. In addition, we represent the cost function evaluated at the solution produced by Algorithm 1, denoted by f^* and the difference between this minimum and the minima computed by SA and SE-Sync, denoted by $\Delta^* = f^* - f$. The CPU time is shown in seconds for all three algorithms.

The three methods benchmarked reach the global optimum in all seven datasets. While there may be disparities regarding precision, the differences in terms of the minimum attained and the set of rotations produced are negligible in the applications considered. We focus thus on the CPU time of each algorithm. Our primal-dual method attains machine precision of λ_1 , and therefore the global optimum, faster than the two other methods take to stop iterating. If we were to relax the upper bound on our stopping criterion, the CPU times could be brought down even further, without compromising the solution as far as geometric reconstructions are concerned. Plots showcasing the convergence of the primal-dual method, in terms of the positive-semidefiniteness of $\Lambda - \tilde{A}$, for four of the datasets are shown in Fig. 5.

8 CONCLUSION

In this paper, we addressed the problem of MLE rotation averaging, as an initialization for PGO in SE(3), or as a stan-

TABLE 1
Comparison between primal-dual iterations (Algorithm 1), Shonan Averaging [4] and SE-Sync [13]. Datasets from [1].

Dataset	Graph		Primal-dual			Shonan averaging			SE-Sync		
	n	m	$ \lambda_1 $	f^*	$t(s)$	$ \lambda_1 $	Δ^* (approx.)	$t(s)$	$ \lambda_1 $	Δ^* (approx.)	$t(s)$
SmallGrid	125	297	10^{-15}	-2118.202	0.02	10^{-07}	-10^{-04}	0.55	10^{-08}	-10^{-05}	0.09
Garage	1661	6275	10^{-15}	-42632.998	0.06	10^{-05}	-10^{-01}	24.5	10^{-14}	-10^{-10}	0.99
Sphere	2200	8647	10^{-15}	-56981.692	0.36	10^{-07}	-10^{-03}	30.1	10^{-09}	-10^{-05}	2.79
Torus3D	5000	9048	10^{-15}	-69227.058	0.35	10^{-06}	-10^{-02}	98.8	10^{-09}	-10^{-05}	3.86
Cubicle	5750	12486	10^{-15}	-92163.079	0.46	10^{-05}	-10^{-02}	96.8	10^{-08}	-10^{-04}	2.49
Grid3D	8000	22236	10^{-15}	-157206.257	1.78	10^{-07}	-10^{-02}	154.54	10^{-09}	-10^{-04}	11.69
Rim	10195	22251	10^{-15}	-164037.930	5.92	10^{-05}	-10^{-01}	221.63	10^{-12}	-10^{-07}	8.73

TABLE 2

Comparison between Primal-dual, Shonan Averaging [24] and the block coordinate descent method (BCD) [9] for random cycle graph problems.

Problem	n	σ (rad)	Primal-dual		Shonan		BCD	
			$ \lambda_1 $	\bar{t} (s)	$\bar{\Delta}^*$	\bar{t} (s)	$\bar{\Delta}^*$	\bar{t} (s)
20	0.2	0.2	10^{-15}	0.019	10^{-4}	0.11	10^{-3}	0.18
		0.5	10^{-15}	0.019	10^{-4}	0.12	10^{-3}	0.23
50	0.2	0.2	10^{-15}	0.020	10^{-3}	0.26	10^{-3}	4.48
		0.5	10^{-15}	0.020	10^{-2}	0.32	10^{-3}	6.80
100	0.2	0.2	10^{-15}	0.022	10^{-2}	0.42	10^{-3}	51.75
		0.5	10^{-15}	0.022	10^{-2}	0.50	10^{-3}	96.19
200	0.2	0.2	10^{-15}	0.024	10^{-2}	0.74	10^{-3}	n.a.
		0.5	10^{-15}	0.024	10^{-1}	1.10	10^{-3}	n.a.

alone problem. We set forth a primal-dual method with spectral updates, and a characterization of stationary points for problems with an underlying cycle graph topology. Our proposed algorithm extends the well-known spectral initialization by updating the dual variable and, as demonstrated by our empirical evaluation, it produces optimal solutions to machine precision in a fraction of the time of existing solvers. Further, it verifies optimality by default at each iteration. We expect this work to open up new avenues of research, namely the extension of the primal-dual iterations to the complete PGO problem in SE(3) and new in terms of new theoretical results regarding the convergence properties of the proposed method.

PROOF OF LEMMA 1

From the update $\Lambda_{(k)}R_{(k+1)} = \tilde{A}R_{(k)}$ write

$$R_{(k+1)}^\top \Lambda_{(k)} R_{(k+1)} = R_{(k+1)}^\top \tilde{A} R_{(k)} \quad (62)$$

Taking the trace on both sides

$$\text{tr}(\Lambda_{(k)}) = \langle R_{(k+1)}, \tilde{A}R_{(k)} \rangle \quad (63)$$

From $\tilde{A}R_{(k+1)} = \Lambda_{(k+1)}R_{(k+2)}$

$$\text{tr}(\Lambda_{(k)}) = \langle R_{(k+2)}, \Lambda_{(k+1)}R_{(k)} \rangle \leq \text{tr}(\Lambda_{(k+1)}) \quad (64)$$

where the inequality arises from the general fact that $\text{tr}(SR) \leq \text{tr}(S)$ for S symmetric and R orthogonal.

PROOF OF LEMMA 2

Start by noting that $\Lambda_{(k)} - \tilde{A} \succeq 0$ is equivalent to $I_{np} - \Lambda_{(k)}^{-\frac{1}{2}} \tilde{A} \Lambda_{(k)}^{-\frac{1}{2}} \succeq 0$ and write the GPM iteration as

$$\Lambda_{(k)}^{\frac{1}{2}} R_{(k+1)} = \left(\Lambda_{(k)}^{-\frac{1}{2}} \tilde{A} \Lambda_{(k)}^{-\frac{1}{2}} \right) \Lambda_{(k)}^{\frac{1}{2}} R_{(k)} \quad (65)$$

Using $\|\Lambda_{(k)}^{\frac{1}{2}} R_{(k+1)}\|_2 = \|\Lambda_{(k)}^{\frac{1}{2}} R_{(k)}\|_2$, the submultiplicative norm property yields

$$\left\| \Lambda_{(k)}^{-\frac{1}{2}} \tilde{A} \Lambda_{(k)}^{-\frac{1}{2}} \right\|_2 \geq 1 \quad (66)$$

Since $A \succeq 0 \implies \Lambda_{(k)}^{-\frac{1}{2}} \tilde{A} \Lambda_{(k)}^{-\frac{1}{2}} \succeq 0$, we have

$$\left\| \Lambda_{(k)}^{-\frac{1}{2}} \tilde{A} \Lambda_{(k)}^{-\frac{1}{2}} \right\|_2 = \lambda_{np} \left(\Lambda_{(k)}^{-\frac{1}{2}} \tilde{A} \Lambda_{(k)}^{-\frac{1}{2}} \right) \quad (67)$$

Thus,

$$\begin{aligned} \lambda_1 \left(I_{np} - \Lambda_{(k)}^{-\frac{1}{2}} \tilde{A} \Lambda_{(k)}^{-\frac{1}{2}} \right) \\ = 1 - \lambda_{np} \left(\Lambda_{(k)}^{-\frac{1}{2}} \tilde{A} \Lambda_{(k)}^{-\frac{1}{2}} \right) \leq 0 \end{aligned} \quad (68)$$

Since the smallest eigenvalue of $I_{np} - \Lambda_{(k)}^{-\frac{1}{2}} \tilde{A} \Lambda_{(k)}^{-\frac{1}{2}}$ is always non greater than zero, the iterations must comprehend infeasible dual estimates.

PROOF OF LEMMA 3

We rewrite the cost function in (20) as

$$f(R) = -2 \sum_{i \sim j} \text{tr}(\tilde{R}_{ij} R_j R_i^\top). \quad (69)$$

Under the hypothesis that the rotations \tilde{R}_{ij} share a common axis, we can restrict our search for R_1, \dots, R_n to this subgroup. Thus, $\angle(\tilde{R}_{ij} R_j R_i^\top) = \angle(\tilde{R}_{ij}) - \angle(R_i R_j^\top)$. From $\text{tr}(R) = 1 + 2 \cos(\angle(R))$, the trace in (69) becomes

$$\text{tr}(\tilde{R}_{ij} R_j R_i^\top) = 1 + 2 \cos(\angle(\tilde{R}_{ij}) - \angle(R_i R_j^\top)). \quad (70)$$

Define the angles $\theta_{ij} := \angle(R_i R_j^\top)$, $\tilde{\theta}_{ij} := \angle(\tilde{R}_{ij})$ and the set $\Theta = \{\theta_{12}, \dots, \theta_{n1}\}$. The optimization problems

$$\begin{aligned} & \underset{\Theta}{\text{maximize}} && \sum_{i \sim j} \cos(\tilde{\theta}_{ij} - \theta_{ij}) \\ & \text{subject to} && \theta_{12} + \dots + \theta_{n1} = 2k\pi, \end{aligned} \quad (71)$$

for $k \in \{0, \dots, n-1\}$, yield stationary points of (20). Let the residuals be $\tilde{\theta}_{ij} - \theta_{ij} \in [-\pi, \pi]$ and let $y \in \mathbb{R}$ be a dual variable. The Lagrangian for (71) is

$$\mathcal{L}(\Theta, y) = \sum_{i \sim j} \cos(\tilde{\theta}_{ij} - \theta_{ij}) + y \left(\sum_{i \sim j} \theta_{ij} - 2k\pi \right) \quad (72)$$

From (72), we have the sufficient stationarity conditions

$$\exists w \in [-\pi, \pi], \forall_{i \sim j} \tilde{\theta}_{ij} - \theta_{ij} = w, \quad (73)$$

$$\exists k \in \{0, \dots, n-1\}, \sum_{i \sim j} \theta_{ij} = 2k\pi. \quad (74)$$

Summing (73) over all the edges of the cycle graph we have

$$\sum_{i \sim j} \tilde{\theta}_{ij} - \sum_{i \sim j} \theta_{ij} = nw. \quad (75)$$

Combining (74) and (75) with $\sum_{i \sim j} \tilde{\theta}_{ij} = \gamma$ yields

$$\theta_{ij} = \tilde{\theta}_{ij} - \gamma/n + 2k\pi/n. \quad (76)$$

From (40), we have $R_i R_j^\top = \tilde{R}_{ij} E_k^\top$, for $i \sim j$. Thus,

$$\angle(R_i R_j^\top) = \angle(\tilde{R}_{ij}) - \angle(E_k) \quad (77)$$

which is simply (76) since $\angle(E_k) = \gamma/n - 2k\pi/n$.

PROOF OF THEOREM 6

We will prove the result for the spectrum of \tilde{A}' , which is equal to that of \tilde{A} since the matrices are similar. We start by showing that the block-vectors $V^k \in \mathbb{R}^{3n \times 3}$, with

$$V^k := \begin{bmatrix} E_k^0 \\ E_k^1 \\ \vdots \\ E_k^{n-1} \end{bmatrix}, \quad (78)$$

indexed by $k \in \{0, \dots, n-1\}$ span invariant subspaces of \tilde{A}' i.e., $\exists H \in \mathbb{R}^{3 \times 3} : \tilde{A}' V^k = V^k H$. For this step, it suffices to compute $\tilde{A}' V^k$. From (49) and (78)

$$\begin{aligned} \tilde{A}' \begin{bmatrix} E_k^0 \\ \vdots \\ E_k^i \\ \vdots \\ E_k^{n-1} \end{bmatrix} &= \begin{bmatrix} E_k^1 + E_k^\top E_k^{n-1} \\ \vdots \\ E_k^{i-1} + E_k^{i+1} \\ \vdots \\ E E_k^0 + E_k^{n-2} \end{bmatrix} \\ &= \begin{bmatrix} E_k^0 \\ \vdots \\ E_k^i \\ \vdots \\ E_k^{n-1} \end{bmatrix} (E_k + E_k^\top). \end{aligned} \quad (79)$$

In compact notation, (79) reads as

$$\tilde{A}' V^k = V^k (E_k + E_k^\top). \quad (80)$$

Since $E_k + E_k^\top \in \mathbb{S}^3$, let its spectral decomposition be

$$E_k + E_k^\top = J \Sigma J^\top, \quad (81)$$

with $J \in O(3)$ and $\Sigma \in \mathbb{R}^{3 \times 3}$ diagonal. From (80) we have

$$\tilde{A}' (V^k J) = (V^k J) \Sigma. \quad (82)$$

The diagonal of Σ contains thus three eigenvalues of \tilde{A}' . From (81), these eigenvalues are those of $E_k + E_k^\top$ i.e., $\{3, 2 \cos(\angle(E_k)), 2 \cos(\angle(E_k))\}$. By definition, $\angle(E_k) = \gamma/n - 2k\pi/n$, thus

$$\{2 \cos(\gamma/n - 2k\pi/n)\}_{k=0, \dots, n-1} \subset \sigma(\tilde{A}), \quad (83)$$

with each eigenvalue having multiplicity 2.

In order to identify the remaining n eigenvalues of \tilde{R} let \hat{n} denote the axis of the cycle error E i.e., $E \hat{n} = \hat{n}$ and $E^\top \hat{n} = \hat{n}$. Define the vectors $z^k \in \mathbb{R}^{3n}$

$$z^k := \begin{bmatrix} 1 \\ \cos\left(\frac{2k\pi}{n}\right) \\ \cos\left(\frac{2k\pi}{n}\right) \\ \vdots \\ \cos\left(\frac{2k\pi}{n}\right) \end{bmatrix} \otimes \hat{n}, \quad (84)$$

indexed by $k \in \{0, \dots, n-1\}$. We have

$$\begin{aligned} \tilde{A}' z^k &= \begin{bmatrix} (\cos\left(\frac{2k\pi}{n}\right) + \cos\left(\frac{2k\pi}{n}\right)) \hat{n} \\ \vdots \\ (\cos\left(\frac{2k\pi}{n}\right) + \cos\left(\frac{2k\pi}{n}\right)) \hat{n} \\ \vdots \\ (\cos\left(\frac{2k\pi}{n}\right) + \cos\left(\frac{2k\pi}{n}\right)) \hat{n} \end{bmatrix} \\ &= \left(2 \cos\left(\frac{2k\pi}{n}\right)\right) \begin{bmatrix} 1 \\ \vdots \\ \cos\left(\frac{2k\pi}{n}\right) \\ \vdots \\ \cos\left(\frac{2k\pi}{n}\right) \end{bmatrix} \otimes \hat{n} \end{aligned} \quad (85)$$

In compact notation, (85) reads as

$$\tilde{A}' z^k = (2 \cos(2k\pi/n)) z^k, \quad (86)$$

for $k \in \{0, \dots, n-1\}$. It follows that

$$\{2 \cos(2k\pi/n)\}_{k=0, \dots, n-1} \subset \sigma(\tilde{A}). \quad (87)$$

Finally, we have

$$\begin{aligned} \sigma(\tilde{A}) &= \{2 \cos(\gamma/n - 2k\pi/n)\}_{k=0, \dots, n-1} \\ &\cup \{2 \cos(2k\pi/n)\}_{k=0, \dots, n-1}. \end{aligned} \quad (88)$$

from combining (83) and (87).

ACKNOWLEDGMENTS

This work was supported by LARSyS funding (DOI: 10.54499/LA/P/0083/2020, 10.54499/UIDP/50009/2020, and 10.54499/UIDB/50009/2020), through Fundação para a Ciência e a Tecnologia. M Marques and J Costeira were also supported by the PT SmartRetail project [PRR - 02/C05-i01.01/2022.PC645440011-00000062], through IAPMEI - Agência para a Competitividade e Inovação.

REFERENCES

- [1] L. Carlone, R. Tron, K. Daniilidis, and F. Dellaert, "Initialization techniques for 3D SLAM: A survey on rotation estimation and its use in pose graph optimization," *Proceedings - IEEE International Conference on Robotics and Automation*, vol. 2015-June, no. June, pp. 4597–4604, 2015.
- [2] L. Carlone, D. M. Rosen, G. Calafiore, J. J. Leonard, and F. Dellaert, "Lagrangian duality in 3D SLAM: Verification techniques and optimal solutions," *IEEE International Conference on Intelligent Robots and Systems*, vol. 2015-Decem, pp. 125–132, 2015.
- [3] R. Kümmerle, G. Grisetti, H. Strasdat, K. Konolige, and W. Burgard, "g2o: A general framework for graph optimization," in *IEEE International Conference on Robotics and Automation*, 2011, pp. 3607–3613.
- [4] F. Dellaert, "Factor graphs and GTSAM: A hands-on introduction," Georgia Institute of Technology, Tech. Rep., 2012.
- [5] R. Hartley, J. Trunpf, Y. Dai, and H. Li, "Rotation averaging," *International journal of computer vision*, vol. 103, no. 3, pp. 267–305, 2013.
- [6] N. Boumal, "Nonconvex Phase Synchronization," vol. 26, no. 4, pp. 2355–2377, 2016.
- [7] J. L. Schonberger and J.-M. Frahm, "Structure-from-motion revisited," in *Proceedings of the IEEE conference on computer vision and pattern recognition*, 2016, pp. 4104–4113.
- [8] R. Tron, R. Vidal, and A. Terzis, "Distributed Pose Averaging in Camera Networks via Consensus on $SE(3)$," in *Proceedings of the 48th IEEE Conference on Decision and Control*, no. 3, 2008.
- [9] A. Eriksson, C. Olsson, F. Kahl, and T. J. Chin, "Rotation Averaging and Strong Duality," *Proceedings of the IEEE Computer Society Conference on Computer Vision and Pattern Recognition*, pp. 127–135, 2018.
- [10] F. Arrigoni, B. Rossi, and A. Fusiello, "Spectral synchronization of multiple views in $SE(3)$," *SIAM Journal on Imaging Sciences*, vol. 9, no. 4, pp. 1963–1990, 2016.
- [11] N. Boumal, "A Riemannian low-rank method for optimization over semidefinite matrices with block-diagonal constraints," pp. 1–36, 2015.
- [12] A. S. Bandeira, N. Boumal, and A. Singer, "Tightness of the maximum likelihood semidefinite relaxation for angular synchronization," *Mathematical Programming*, vol. 163, no. 1-2, pp. 145–167, 2017.
- [13] D. M. Rosen, L. Carlone, A. S. Bandeira, and J. J. Leonard, "SE-Sync: A certifiably correct algorithm for synchronization over the special Euclidean group," *International Journal of Robotics Research*, vol. 38, no. 2-3, pp. 95–125, 2019.
- [14] G. Moreira, M. Marques, and P. Costeira, "Rotation Averaging in a Split Second : A Primal-Dual Method and a Closed-Form for Cycle Graphs," in *International Conference on Computer Vision*, 2021.
- [15] C. Sidhartha and V. M. Govindu, "It is all in the weights: Robust rotation averaging revisited," in *2021 International Conference on 3D Vision (3DV)*. IEEE, 2021, pp. 1134–1143.
- [16] P. Purkait, T.-J. Chin, and I. Reid, "Neurora: Neural robust rotation averaging," in *European Conference on Computer Vision*. Springer, 2020, pp. 137–154.
- [17] S. H. Lee and J. Civera, "Hara: A hierarchical approach for robust rotation averaging," in *Proceedings of the IEEE/CVF Conference on Computer Vision and Pattern Recognition*, 2022, pp. 15777–15786.
- [18] N. Boumal, A. Singer, P. A. Absil, and V. D. Blondel, "Cramér-Rao bounds for synchronization of rotations," *Information and Inference*, vol. 3, no. 1, pp. 1–39, 2014.
- [19] J. R. Peters, D. Borra, B. E. Paden, and F. Bullo, "Sensor network localization on the group of three-dimensional displacements," *SIAM Journal on Control and Optimization*, vol. 53, no. 6, pp. 3534–3561, 2015.
- [20] K. J. Doherty, D. M. Rosen, and J. J. Leonard, "Performance guarantees for spectral initialization in rotation averaging and pose-graph slam," *arXiv preprint arXiv:2201.03773*, 2022.
- [21] G. Moreira, M. Marques, and J. Paulo Costeira, "Fast Pose Graph Optimization via Krylov-Schur and Cholesky Factorization," in *IEEE/CVF Proceedings of the Winter Conference on Applications of Computer Vision*, 2021, pp. 1898–1906. [Online]. Available: <https://github.com/gabmoreira/maks>
- [22] H. Liu, M.-c. Yue, and A. M.-C. So, "On the Estimation Performance and Convergence Rate of the Generalized Power Method for Phase Synchronization," *SIAM Journal on Optimization*, vol. 27, no. 4, pp. 2426–2446, 2017.
- [23] S. Burer and R. D. Monteiro, "A nonlinear programming algorithm for solving semidefinite programs via low-rank factorization," *Mathematical Programming, Series B*, vol. 95, no. 2, pp. 329–357, 2003.
- [24] F. Dellaert, D. M. Rosen, J. Wu, R. Mahony, and L. Carlone, "Shonan Rotation Averaging: Global Optimality by Surfing $SO(p)^n$," in *European Conference on Computer Vision*, vol. 12351 LNCS, no. 1, 2020, pp. 292–308.
- [25] N. Boumal, A. Singer, P. A. Absil, and V. D. Blondel, "Cramér-Rao bounds for synchronization of rotations," *Information and Inference*, vol. 3, no. 1, pp. 1–39, 2014.
- [26] B. Gao, X. Liu, and Y. Yuan, "Parallelizable algorithms for optimization problems with orthogonality constraints," *SIAM Journal on Scientific Computing*, vol. 41, no. 3, pp. A1949–A1983, 2019.